Powder Diffraction
Paper (final)
November 2, 2015

X-ray powder diffraction characterization of the large volume unit-cell of the M8 murataite polytype

Ryosuke S. S. Maki,[a] Peter E. D. Morgan,[b] and Yoshikazu Suzuki[a, c*]

[a] Graduate School of Pure and Applied Sciences, University of Tsukuba, Tsukuba, Ibaraki 305-8573, Japan

[b] Department of Chemical Engineering and Materials Science, University of California Irvine, CA 92697, USA

[c] Faculty of Pure and Applied Sciences, University of Tsukuba, Tsukuba, Ibaraki, 305-8573, Japan

Abstract

We have used conventional X-ray powder diffraction to study one of the largest volume inorganic mixed oxide unit supercell structures done so far. This necessitated some SAXS-like observations at low angles from < 2° 2θ to concord with electron diffraction, which had indicated an 8×8×8 huge volume supercell of a fluorite-type basic sub-cell. Emphasis is on the detection of, possibly very weak, fingerprint, low-angle/long lines/peaks which will indicate the (often unsuspected) presence of complex polytypic arrangements of simple very strong basic sub-cells and so facilitate synthetic studies.

Key words: murataite, SAXS, fluorite-type basic sub-cell, tranquillityite, YBO_3.

[*] Corresponding Author
Faculty of Pure and Applied Sciences, University of Tsukuba,
1-1-1 Tennodai, Tsukuba, Ibaraki, 305-8573, Japan
E-mail: suzuki@ims.tsukuba.ac.jp
Tel: +81-29-853-5026 / Fax: +81-29-853-4490

I. INTRODUCTION

It is perhaps astonishing to have synthesized, by the standard ceramic procedure of co-firing oxides, an ~90% pure very complex oxide crystal type containing Al, Ca, Fe, Mn, Ti, and Zr, with an enormous FCC unit cell with a = 39.269 Å units. It is a member of the pyrochlore-murataite modular polysomatic family (Urusov *et al.*, 2007) with an eightfold supercell of a fluorite-type basic sub-cell *viz.* M8, (i.e. containing 8×8×8 = 512 basic sub-cells, about 5,250 atoms and 40 distinct symmetry cation positions, (Laverov *et al.*, 2006, 2011a)).

The first member of this group, now dubbed M3, (nearly) isotypic with the natural mineral, murataite (Adams *et al.*, 1974), was discovered during research on radwaste disposal, in a mixture with many cations, (PDF 00-036-0138 (ICDD, 1982)). It was recognized as a 3×3×3 fluorite supercell (structurally very similar to the mineral murataite, M, but with a surprisingly very different elemental content) (Morgan and Ryerson, 1982; Morgan *et al.*, 1984). The detailed crystal structure was published much later (Pakhomova *et al.*, 2013).

The well-known 2×2×2 cousin is pyrochlore, Py, also frequently considered for radwaste disposal. Subsequently in a superior research effort in Russia, aimed specifically at radwaste disposal, it was discovered that there were a series of modular polytypes between Py and M, such as M5, M7, M8, in addition to M3 (Laverov *et al.*, 1999); other packing variants are probably yet, likely soon, to be revealed. Moon tranquillityite brought during the Apollo 11 mission (Gatehouse *et al.*, 1977), was initially amorphous, but now appears plausibly to be one of these. The regions connecting the fluorite-type sub-cells can vary in fine detail.

The new polytypes, identified by very careful electron diffraction, were first achieved by melt methods; these produced good-sized crystals but with zoning (a downside for single crystal XRD but a plus for radwaste entombment). The polytypes are most routinely made by simple mixed oxide firings, whereupon, the X-ray powder diffraction (XRPD) method is the method of choice for simplicity and speediness in monitoring exactly how a day-to-day synthesis program may be proceeding, bearing in mind the many variables, of about 6 cation content ratios, the temperatures and times of syntheses and so forth.

Very large unit-cells turn out to be much more difficult to analyze with advanced powder methods, such as a Rietveld method; analysis on the largest oxide unit cell attempted so far (only 3 cations), was published as $La_3Ti_5Al_{15}O_{37}$ (Morris *et al.*, 1994). It was later corrected to the originally proposed $LaTi_2Al_9O_{19}$ (Morgan, 1984) with the aid of the subsequent single crystal determination of isomorphous $SrTi_3Al_8O_{19}$ (Strunk and Müller-Buschbaum, 1993) and checked (as always required today) with bond-valence sums (Kasunič *et al.*, 2011). The unit-cell considered here, with 6 or more cations in a mixed oxide, is much larger by volume, in fact about three times larger, than an inorganic one previously referred to as "a giant unit-cell" (Aliev *et al*., 2014).

The natural mineral, an M3, (Ercit and Hawthorne, 1995) is known to contain many defects that include mixed polytypic layers and this probably applies to the "reconstituted-by-heating" tranquillityite (Gatehouse *et al.*, 1977). In addition, the main diffraction peaks of the supercells, derived from the similar basic sub-cells, means, close overlaps occur for all the polytypes at all the strongest peaks (Laverov *et al.*, 2011b). Therefore, for quick analysis, we need accurate XRPD patterns especially emphasizing the lowest angle lines where these complex polytypes are most readily distinguishable.

The first possible FCC line/peak of M8, the (111), would be expected at about $2\theta = 3°$, so special steps must be taken to enable searching at unusually low 2θ angles by masking the background - mimicking a small-angle X-ray scattering (SAXS) technique. Other modular types, with lower symmetry, could produce even lower angle lines. We present here the XRPD for M8, found to be FCC as predicted, (Laverov *et al.*, 2011a), exemplifying the ease of indexing and unit-supercell confirmation. Quote:- "From the crystal chemical point of view, the murataite series are the most complex mixed oxides known to date" (Laverov *et al.*, 2011a).

II. EXPERIMENTAL

Commercial α-Al_2O_3 (99.99% purity, Taimei Chemicals Co. Ltd., Saitama, Japan), TiO_2 anatase (99% purity, Kojundo Chemical Laboratory Co. Ltd.), CaO (99.9% purity, Kojundo Chemical Laboratory Co. Ltd.), MnO_2 (99% purity, Kojundo Chemical Laboratory Co. Ltd.), ZrO_2 (98% purity, Kojundo Chemical Laboratory Co. Ltd.) and

α–Fe_2O_3 (99.9% purity, Wako Pure Chemical Industries Ltd.) powders were used as starting materials. The starting powders, α-Al_2O_3 : CaO : TiO_2 : MnO_2 : α-Fe_2O_3 : ZrO_2 = 6.4 : 9.6 : 37.7 : 7.1 : 17.1 : 22.1 in wt.%, (viz. 5.8 : 16.0 : 43.9 : 7.6 : 10.0 : 16.7 in mol.%), were mixed by planetary ball-milling with ZrO_2 media for 30 min (acceleration: 4*g*). The powder mixtures were sieved through a 150-mesh screen. Cylindrical pellet (diameter of 15 mm) was prepared by the uniaxial cold isostatic pressing (CIP) of the mixed oxides at 200 MPa for 10 min. The green sample was then sintered at 1300°C for 6 h in air in an alumina crucible coated with Pt foil.

Transmission electron microscope-selected area electron diffraction pattern (TEM-SAED) of the crushed sample was observed by aberration-corrected transmission electron microscopy (JEOL, JEM-2200FS, operated at 200 kV), in order to discover the superstructure of this particular murataite. The atomic composition on a polished section of the bulk sample was measured by scanning electron microscopy (Hitachi TM3000, operatedd at 15 kV) equipped with energy dispersive X-ray spectrometry (SEM-EDS).

The phases in the pulverized sample were analyzed by XRPD (Rigaku Multiflex counter diffractometer with graphite-monochromatized Cu-$K_{\alpha 1\alpha 2}$ radiation ($\lambda_{Cu\text{-}K\alpha 1}$=1.54056 Å, $\lambda_{Cu\text{-}K\alpha 2}$=1.54439 Å), operated at 40 kV and 40 mA, 27°C), using a reflection-free single-crystal silicon stage. The slit sizes of divergence slit (DS), scatter slit (SS) and receiving slit (RS) were 1°, 1° and 0.15 mm, respectively. Very slow step scans (step: 0.01°) were done with the scan time of 70 s/step in a range of 2θ=2–10° with judicious masking of the incident beam and background forward scatter. A normal scan (*viz.* without masking) was done with the scan time of 30 s/step in a range of 2θ = 9–50°, and with the scan time of 20 s/step in a range of 2θ = 50–150° with the background removed. *K*α_2 lines were removed by the Rachinger algorithm.

The peak search was carried out with peak search algorithm based on Savitzky-Golay method in powder pattern integrated analysis software (JADE7, RIGAKU, Japan). A fully automatic peak search software, however, has the possibility of failure in detecting the weak peaks; the murataite phase contains large numbers of weak peaks from the supercell (i.e. superlattice reflections); these supercell peaks were manually searched. All indices and the relative intensities were manually calculated

without using any specific software.

III. RESULTS AND DISCUSSION

TEM-SAED (Figure 1) revealed that the murataite phase had an 8×8×8 (M8) superstructure. Indexing for all peaks of the murataite phase were carried out mostly manually, securely aware of this.

SEM-EDS analyses (Table I) measured the atomic ratio of each element. The pseudobrookite (P)-type phase, containing much Al, Ti and Fe element, agrees well with the conventional formula. We concur that Mn in the starting material is an essential condition for synthetic M formation (Laverov *et al.*, 1999), where it may reside in trigonal bipyramids (as it often prefers e.g. in $YMnO_3$, as Mn^{3+} (Aken *et al.*, 2001)). Moreover Mn, is known also to aid in the formation of tranquillityite (Gatehouse *et al.*, 1977), another reason that we think it has similarities in this extended polytypic group. M8 has 2 α-Keggin groups with an AlO_4 tetrahedron at its center (Laverov *et al.*, 2011a), resulting in the higher Al contents in M8 than in zirconolite (Z).

In Table I, Z's composition is quite like M8 but with a little less Al, and P's composition is quite similar to M8 but with more iron and less zirconium. Reaction appears to be incomplete because the contents of the Z and P sum to about the same composition as the M8. With six elements, it is almost certain that, at 1300°C, a liquid formed from which, on cooling, Z and P crystallized and which facilitated the good crystallization of M8 as micrographic observations (to be published elsewhere).

Figure 2, 3 and Table I revealed that the resultant phases after sintering were about 90% major M8, about 5% minor $(Fe,Al,Mg)_2(Ti,Zr)O_5$ P, and about 5% minor $(Ca,Mn)ZrTi_2O_7$-2M Z, (PDF 00-041-1432 and 00-034-0167 (ICDD, 1988 and 1982)). In the present work, the XRPD pattern was collected in three distinct 2θ ranges, with specific experimental conditions in each of them.

The XRPD indexing (Table II) confirms that M8 is FCC, with (*h k l*) all odd or all even. Low angle lines are well visible but with the noticeable absence of the (1 1 1), for which there seems not to be any systematic reason, and we do not believe it is smothered by the background. M8 conforms also to the extra condition (*h* 0 0) where *h* = 4*n* only, consequently, and especially noticeable, leading to the absence of the (2 0 0).

This allows for four space groups (SGs), $Fd\bar{3}$(203), $F4_132$ (210), $Fd\bar{3}m$ (227) and $Fd3c$ (228). Three of these SGs have (*h k* 0) where $h+k = 4n$ only, but we do find the (6 4 0) and (12 2 0), without overlaps, to be present, thus leaving only $F4_132$ (210), not the same SG of $F4\bar{3}m$ (216) as for M3.

The lattice constant was calculated by using only the strong certain reflections at high angles [(32 0 0), (24 24 8), (32 16 0), (32 16 16), (40 8 8), (32 32 0), (40 24 8) and (48 0 0)] - where all the (*h k l*) are divisible by 8, i.e. those from the FCC basic sub-cell. The lattice constant, *a*, of the M8 superstructure is 39.269±0.001 Å, calculated using a Nelson–Riley extrapolation.

Here there is no rare earth so those elements are not mandatory but can play a role as they do in the work of Laverov *et al.* The full range of elements that will enter these structures is to be determined but appears to be most of the periodic table excepting, perhaps, the very largest ions - making them especially interesting for long-term radwaste sequestration.

IV. SUPPLEMENTAL COMMENT

There is considerable risk when not observing possible low angle very weak peaks, especially as we move to these more complex materials. One particularly “good” example hampered the (maybe overspecialized) applied luminescent/fluorescent community; these researchers published well over 70 papers that maintained that YBO_3, and its isotypes, were “vaterites” (isotypic with a form of $CaCO_3$) and/or had hexagonal symmetry – this was actually the strong basic sub-cell with B hardly contributing to the intensities. Low angle very weak peaks would have revealed the larger monoclinic 2-layer pseudowollastonite cell, isotypic with $CaSiO_3$, (pseudowollastonites are notorious for having polytypic complexity, Morgan *et al*., 1977; Yang and Prewitt, 1999); unawareness of the true unit-cells, or intergrowths thereof, quite possibly might partly explain some variable luminescence results. Single crystal work was necessary, coming to the rescue (Lin *et al.*, 2004; Pitscheider *et al.*, 2011) even though the powder technique had, indeed, much earlier flagged the problem (Morgan *et al*., 1977). Although Lin *et al*. identified the correct monoclinic cell, they were unaware that it is a known pseudowollastonite-type.

For routine “fingerprinting”, slow scans only from ~2° to 15-20° may be sufficient. Higher intensity sources would be beneficial, but, may not be available on a day-to-day basis. A rotating stage would also help as so many planes must orient in the diffraction mode.

This approach should be applied to M5 and M7 (M3 already done) so as to provide the engineering synthesizer a speedier monitoring to gauge progress in his/her efforts with so many possible cations. Likely other families of very complex polytypes may be discovered more quickly as ceramics style efforts pursue evermore complex cationic mixes for novel/exotic physical properties.

V. CONCLUSION

(1) M8 has been synthesized remarkably pure by the simple standard ceramic procedure of co-firing oxides. Its XRPD contains more than the 239 surely identified lines.

(2) The M8 superstructure was first observed by TEM-SAED enabling the analysis by the powder method with some confidence. The calculated lattice constant, *a*, of this M8 superstructure is 39.269(1) Å; it is most likely the largest inorganic mixed-oxide unit-cell ever studied by somewhat conventional powder diffraction.

(3) Systematic extinctions of all *(h 0 0)*, where $h \neq 4n$, and the existence of some *(h k 0)* peaks, where $h+k \neq 4n$, suggests it belongs in the SG, $F4_132$ (210), contrasting with an earlier suggestion that the SG might be $F4\bar{3}m$ (216). Some random varying site occupancies of the cations would, in any case, make assigning an ideal SG impossible.

ACKNOWLEDGMENTS

The authors thank the National Institute for Material Science (NIMS) for the use of SEM-EDS. We also appreciate to the Institute for Chemical Research, Kyoto University for the help of TEM-SAED analysis. Detailed work of these techniques will be published later.

REFERENCES

Adams, J. W., Botinelly, T., Sharp, W. N., and Robinson, K. (**1974**). "Murataite, a new complex oxide from El Paso County, Colorado," Am. Mineral. **59**, 172-176.

Aken, B. B. V., Meetsma, A., and Pastra, T. T. M. (**2001**). "Hexagonal $YbMnO_3$ revisited," Acta Cryst. **57**, i87-i89.

Aliev, A., Kovrugin, V. M., Colmont, M., Terryn, C., Huve, M., Siidra, O. I., Krivovichev, S. V., and Mentre, O. (**2014**). "Revised bismuth chloroselenite system: evidence of a non-centrosymmetric structure with a giant unit cell," Cryst. Growth Des. **14**, 3026-3034.

Ercit, T. S., and Hawthorne, F. C. (**1995**). "Murataite, a UB_{12} derivative structure with condensed kegging molecules," Can. Mineral. **33**, 1223-1229.

Gatehouse, B. M., Grey, L. N., Lovering, J. F., and Wark, D. A. (**1977**). "Structure studies on tranquillityite and related synthetic phases," Proc. Lunar. Sci. Conf. **2**, 1831-1838.

Kasunič, M., Meden, A., Škapin, S. D., Suvorov, D. and Golobič, A. **(2011).** "Structure of $LaTi_2Al_9O_{19}$ and reanalysis of the crystal structure of $La_3Ti_5Al_{15}O_{37}$," Acta Cryst. **B67**, 455-460.

Laverov, N. P., Yudintsev, S. V., Omel'yanenko, B. I., Nikonov, B. S., Stefanovskii, S. V. (**1999**). "Murataite ceramics for the immobilization of actinides," Geol. Ore Deposits **41**, 85-93.

Laverov, N. P., Yudintsev, S. V., Stefanovsky, S. V., Omel'yaneko, B. I., and Nikonov, B. S. (**2006**). "Murataite as a universal matrix for immobilization of actinides," Geol. Ore Deposits **48**, 335-356.

Laverov, N. P., Urusov, V. S., Krivovichev, S. V., Pakhomova, A. S., Stefanovsky, S. V., and Yudintsev, S. V. (**2011a)**. "Modular Nature of the Polysomatic Pyrochlore-Murataite Series," Geol. Ore Deposits **53**, 273–294.

Laverov, N. P., Yudintsev, S. V., Stefanovskii, S. V., Omel'yanenko, B. I., and Nikonov, B. S. (**2011b**). "Murataite matrices for actinide wastes," Radiochemistry **53**, 229-243.

Lin, J., Sheptyakov, D., Wang, Y., and Allenspach, P., (**2004**). "Structures and phase transition of vaterite-type rare earth orthoborates: a neutron diffraction study," Chem. Mater. **16**, 2418-2424.

Morgan, P. E. D., Carrol, P. J., and Lange, F. F. (**1977**). “Crystal structure of $YSiO_2N$ and a reappraisal of the “vaterite” type, YBO_3,” Mater. Res. Bull. **12**, 251-260.

Morgan, P. E. D., and Ryerson, F. J. (**1982**). “A new “cubic” crystal compound,” J. Mater. Sci. Lett. **1**, 351-352.

Morgan, P. E. D., Harker, A. B., and Flintoff, J. F. (**1984**). “Developments in SRP "composite" defense ceramic radwaste forms,” Adv. Ceram. **8**, 234-246.

Morgan, P. E. D. (**1984**). “Preparing new extremely difficult-to-form crystal structures,” Mater. Res. Bull. **19**, 369–376.

Morris, R. E., Owen, J. J., Stalick, J. K., and Cheetham, A. K. (**1994**). “Determination of Complex Structures from Powder Diffraction Data: The Crystal Structure of $La_3Ti_5Al_{15}O_{37}$,” J. Solid State Chem. **111**, 52-57.

Pakhomova, A. S., Krivovichev, S. V., Yudintsev, S. V., and Stefanovsky, S. V. (**2013**). “Synthesis murataite-3C, a complex form for long-term immobilization of nuclear waste: crystal structure and its comparison with natural analogues,” Z. Kristallogr. **228**, 151-156.

Pitscheider, A., Kaindl, R., Oeckler, O., and Huppertz, H. (**2011**). “The crystal structure of π–$EuBO_3$: new single-crystal data for an old problem,” J. Solid State Chem. **184**, 149-153.

Strunk, M., and Müller-Buschbaum, V. (**1993**). “Zur kristallstruktur von $SrAl_8Ti_3O_{19}$,” J. Alloy Compd. **198**, 101-104.

Urusov, V. S., Organova, N. I., Karimova, O. V., Yudintsev, S. V., and Ewing, R. C. (**2007**). “A modular model of the crystal structure of the pyrochlore-murataite polysomatic series,” Crystallogr. Rep. **52**, 37-46.

Yang, H., and Prewitt, C. T. (**1999**). “On the crystal structure of pseudowollastonite ($CaSiO_3$),” Am. Mineral. **84**, 929-932.

Tables

TABLE I. Chemical compositions (EDS) of the coexisting phases in the sintered sample.

Oxide (wt. %)	M8	Pseudobrookite	Zirconolite
Al_2O_3	5.9	9.9	2.7
CaO	9.3	2.4	10.2
TiO_2	37.7	39.7	36.9
MnO_2	6.3	6.4	3.1
Fe_2O_3	14.9	32.8	7.9
ZrO_2	25.9	8.8	39.3

TABLE II**.** Detailed list of X-ray diffraction peaks of M8 sample. There are a total of 239, mostly very weak FCC lines, from the supercell, 13 stronger FCC lines come from the fluorite-type basic sub-cell. In the case of many overlapping values of $h^2+k^2+l^2$, we choose, for simplicity, to show only the one with the lowest value of l (marked with the "+" symbol).

$2\theta_{obs}$	d_{obs} (Å)	I/I_0	*hkl*	$2\theta_{calc}$	d_{calc} (Å)	$2\theta_{obs}$-$2\theta_{calc}$
6.37	13.862	4.2	2 2 0	6.36	13.884	0.01
7.48	11.811	6.0	3 1 1	7.46	11.840	0.02
7.81	11.311	5.1	2 2 2	7.79	11.336	0.02
9.01	9.807	6.9	4 0 0	9.00	9.817	0.01
9.82	9.000	4.7	3 3 1	9.81	9.009	0.01
11.01	8.029	6.6	4 2 2	11.03	8.016	-0.02
11.70	7.558	10.0	5 1 1 +	11.70	7.557	0.00
13.29	6.657	5.6	5 3 1	13.33	6.638	-0.04
14.23	6.219	7.2	6 2 0	14.25	6.209	-0.02
15.66	5.654	7.2	4 4 4	15.62	5.668	0.04
15.92	5.562	6.9	5 5 1	16.11	5.499	-0.19
16.06	5.514	7.9	6 4 0	16.26	5.446	-0.20
16.93	5.233	6.9	6 4 2	16.88	5.248	0.05
19.16	4.629	19.3	6 6 0 +	19.16	4.628	0.00
19.56	4.535	9.3	7 5 1 +	19.56	4.534	0.00
21.18	4.191	6.9	6 6 4	21.21	4.186	-0.03
22.45	3.957	12.0	7 7 1 +	22.51	3.947	-0.06
23.45	3.791	7.3	10 2 2 +	23.52	3.779	-0.07
25.09	3.546	6.9	7 7 5	25.13	3.541	-0.04
26.50	3.361	6.6	8 6 6 +	26.45	3.367	0.05
26.81	3.323	8.0	10 6 2	26.84	3.319	-0.03
27.24	3.271	10.6	12 0 0 +	27.23	3.272	0.01
27.51	3.240	9.6	11 5 1 +	27.52	3.239	-0.01
27.60	3.229	12.2	12 2 0	27.61	3.228	-0.01
28.24	3.158	5.3	11 5 3 +	28.27	3.154	-0.03

28.76	3.102	4.9	12 4 0	28.73	3.105	0.03
29.11	3.065	6.6	12 4 2 +	29.10	3.066	0.01
29.73	3.003	6.6	13 1 1 +	29.73	3.003	0.00
30.73	2.907	57.0	12 6 2	30.86	2.895	-0.13
31.54	2.834	1000.0	8 8 8 * #	31.54	2.834	0.00
32.16	2.781	41.6	10 10 0 +	32.21	2.777	-0.05
33.52	2.671	5.9	14 4 2 +	33.51	2.672	0.01
34.34	2.609	5.9	15 1 1 +	34.38	2.606	-0.04
35.03	2.559	4.9	15 3 1	35.00	2.562	0.03
35.61	2.519	8.2	11 11 1+	35.61	2.519	0.00
36.58	2.455	116.0	16 0 0 *	36.58	2.454	0.00
36.82	2.439	14.0	13 9 3 +	36.80	2.440	0.02
37.38	2.404	14.0	11 11 5 #+	37.39	2.403	-0.01
37.54	2.394	14.0	14 6 6 +	37.46	2.399	0.08
37.77	2.380	6.9	16 4 4 +	37.75	2.381	0.02
37.97	2.368	5.9	15 7 1 +	37.97	2.368	0.00
38.32	2.347	7.6	12 10 6	38.32	2.347	0.00
38.86	2.316	4.3	12 12 0 +	38.89	2.314	-0.03
39.54	2.277	11.0	14 10 0 +	39.45	2.283	0.09
39.66	2.271	14.6	13 11 3 +	39.65	2.271	0.01
40.65	2.218	10.0	17 5 1 +	40.75	2.213	-0.10
41.24	2.187	10.0	17 5 3 +	41.28	2.185	-0.04
41.36	2.181	19.3	16 8 2 #+	41.35	2.182	0.01
42.08	2.146	4.3	16 8 4	42.15	2.142	-0.07
42.29	2.135	6.6	13 13 1 +	42.34	2.133	-0.05
42.67	2.117	9.2	14 12 2 +	42.67	2.117	0.00
42.86	2.108	27.6	15 11 1 #+	42.86	2.108	0.00
43.39	2.084	7.6	15 11 3 +	43.38	2.084	0.01
43.87	2.062	31.3	19 1 1 #+	43.89	2.061	-0.02
44.50	2.034	7.6	16 10 4	44.46	2.036	0.04
45.25	2.002	7.2	16 8 8	45.21	2.004	0.04

45.73	1.983	5.3	14 14 0 +	45.71	1.983	0.02
45.94	1.974	7.6	14 14 2 +	45.95	1.973	-0.01
46.17	1.965	15.0	16 12 0 +	46.20	1.963	-0.03
46.68	1.944	5.7	20 2 2 +	46.68	1.944	0.00
47.31	1.920	4.9	17 11 3 +	47.35	1.918	-0.04
48.01	1.893	7.2	18 10 2 +	47.88	1.898	0.13
48.30	1.883	6.9	17 11 5 +	48.30	1.883	0.00
48.61	1.871	4.6	20 6 2 +	48.59	1.872	0.02
49.26	1.848	21.9	15 15 1 +	49.24	1.849	0.02
49.52	1.839	9.9	16 14 2 +	49.53	1.839	-0.01
50.56	1.804	15.0	21 5 3 +	50.62	1.802	-0.06
50.90	1.793	30.9	20 8 4	50.90	1.792	-0.01
51.53	1.772	8.9	21 7 1 +	51.53	1.772	0.00
51.86	1.762	8.9	21 7 3 +	51.98	1.758	-0.12
52.46	1.743	21.0	19 11 5 +	52.42	1.744	0.04
52.71	1.735	345.7	16 16 0 *#	52.70	1.735	0.01
52.86	1.731	53.0	7 15 1 +	52.87	1.730	-0.01
53.14	1.722	12.0	18 14 0 +	53.14	1.722	0.00
53.35	1.716	9.6	18 14 2 +	53.36	1.716	-0.01
53.58	1.709	9.6	16 16 4 +	53.58	1.709	0.00
53.98	1.697	5.9	18 14 4 +	54.02	1.696	-0.04
54.16	1.692	6.6	23 3 1 +	54.18	1.691	-0.02
54.62	1.679	6.3	23 3 3 +	54.62	1.679	0.00
55.31	1.660	6.3	20 12 4	55.32	1.659	-0.01
56.43	1.629	9.0	20 12 6 +	56.38	1.631	0.05
56.60	1.625	7.0	22 10 0 +	56.59	1.625	0.01
57.42	1.604	8.0	20 14 2 +	57.43	1.603	-0.01
57.96	1.590	6.3	21 13 1 +	58.01	1.589	-0.05
58.44	1.578	5.9	21 13 3 +	58.42	1.578	0.02
59.68	1.548	7.7	24 8 2 +	59.71	1.547	-0.03
59.85	1.544	9.6	18 18 0 +	59.86	1.544	-0.01

60.35	1.533	23.0	20 16 0 +	60.32	1.533	0.03
60.47	1.530	16.0	23 11 3 +	60.47	1.530	0.00
60.76	1.523	7.0	18 18 4 +	60.72	1.524	0.04
61.21	1.513	9.6	25 7 1 +	61.28	1.511	-0.07
61.51	1.506	16.0	22 14 0 +	61.53	1.506	-0.02
61.71	1.502	6.6	22 14 2 +	61.73	1.502	-0.02
61.97	1.496	7.2	20 12 12	61.93	1.497	0.04
62.73	1.480	193.8	24 8 8 *	62.73	1.480	0.00
62.92	1.476	22.0	16 16 14	62.92	1.476	0.00
63.18	1.470	12.9	26 6 0 +	63.12	1.472	0.06
63.68	1.460	6.0	19 19 1 +	63.66	1.460	0.02
64.05	1.453	16.0	21 17 1 +	64.06	1.452	-0.01
65.24	1.429	7.2	23 15 1 +	65.23	1.429	0.01
65.87	1.417	48.9	16 16 16 *#	65.86	1.417	0.01
66.09	1.413	8.0	22 12 12 +	66.05	1.413	0.04
66.26	1.409	6.0	26 10 0 +	66.24	1.410	0.02
66.78	1.400	5.3	27 7 3 +	66.77	1.400	0.01
67.53	1.386	6.6	21 19 1 +	67.54	1.386	-0.01
68.31	1.372	6.6	23 17 1 +	68.30	1.372	0.01
69.10	1.358	5.3	24 16 2 +	69.10	1.358	0.00
69.83	1.346	5.3	25 15 1 +	69.81	1.346	0.02
70.19	1.340	6.3	25 15 3 +	70.19	1.340	0.00
70.94	1.327	7.3	29 5 3 +	70.93	1.328	0.00
71.33	1.321	4.9	21 21 1 +	71.31	1.322	0.02
71.68	1.316	4.9	23 19 1 +	71.68	1.316	0.00
72.33	1.305	6.6	30 2 0 +	72.28	1.306	0.05
73.23	1.291	5.6	21 9 1 +	73.16	1.293	0.07
73.89	1.282	4.3	25 17 5 +	73.89	1.282	0.00
75.01	1.265	4.3	29 11 1 +	74.99	1.265	0.02
75.37	1.260	6.6	23 21 1 +	75.36	1.260	0.01
76.14	1.249	6.9	25 19 1 +	76.09	1.250	0.05

76.56	1.243	5.3	28 14 4 +	76.49	1.244	0.07
76.82	1.240	4.9	27 15 7 +	76.81	1.240	0.01
77.17	1.235	8.2	29 13 1 +	77.17	1.235	0.00
77.77	1.227	25.6	32 0 0 *	77.76	1.227	0.01
77.94	1.225	11.9	28 12 10 +	77.94	1.225	0.00
78.49	1.218	5.3	28 16 0 +	78.48	1.218	0.01
78.99	1.211	4.3	31 9 3 +	78.98	1.211	0.01
79.25	1.208	3.6	28 16 4 +	79.20	1.208	0.05
79.76	1.201	3.3	22 22 10 +	79.74	1.202	0.02
80.07	1.197	3.6	25 21 3 +	80.05	1.198	0.02
80.47	1.193	3.3	31 11 1 +	80.41	1.193	0.06
80.94	1.187	4.6	30 14 0 +	80.99	1.186	-0.05
81.54	1.180	4.0	30 12 8 +	81.53	1.180	0.01
81.73	1.177	3.0	28 18 2 +	81.70	1.178	0.03
82.42	1.169	4.6	32 10 2 +	82.42	1.169	0.00
82.90	1.164	5.6	33 7 1 +	82.91	1.164	-0.01
83.10	1.161	5.9	28 18 6 +	83.13	1.161	-0.03
83.91	1.152	3.6	25 23 3 +	83.97	1.152	-0.06
84.72	1.143	4.6	27 21 3 +	84.68	1.144	0.04
85.10	1.139	4.6	28 20 2 +	85.08	1.139	0.02
85.41	1.136	4.9	31 15 3 +	85.39	1.136	0.02
85.84	1.131	5.9	32 12 6 +	85.79	1.132	0.05
86.32	1.126	59.8	24 24 8 *	86.32	1.126	0.00
87.12	1.118	5.3	35 3 1 +	87.16	1.117	-0.04
87.54	1.114	6.9	35 3 3 +	87.51	1.114	0.03
88.25	1.106	4.6	34 10 2 +	88.26	1.106	-0.01
89.15	1.098	33.2	32 16 0 *	89.14	1.098	0.01
89.86	1.091	6.9	36 0 0 +	89.85	1.091	0.01
90.16	1.0878	5.6	30 20 2 +	90.20	1.0875	-0.04
90.69	1.0829	5.3	33 15 1 +	90.68	1.0829	0.01
91.02	1.0798	4.9	31 19 1 +	91.04	1.0796	-0.02

91.46	1.0757	5.3	28 22 8 +	91.43	1.0760	0.03
91.84	1.0723	4.6	33 15 5 +	91.74	1.0732	0.10
92.46	1.0667	5.3	27 25 1 +	92.45	1.0668	0.01
93.12	1.0609	5.6	29 23 1 +	93.15	1.0606	-0.03
93.58	1.0569	5.9	32 16 10 +	93.55	1.0571	0.03
93.81	1.0549	4.6	33 17 3 +	93.86	1.0544	-0.05
94.33	1.0504	4.6	36 10 2 +	94.44	1.0495	-0.11
94.55	1.0486	4.9	31 21 1 +	94.57	1.0484	-0.02
94.97	1.0450	5.6	36 10 4 +	94.97	1.0451	0.00
95.25	1.0427	5.3	37 7 1 +	95.28	1.0425	-0.03
95.69	1.0391	5.9	32 20 2 +	95.68	1.0392	0.01
96.43	1.0331	6.3	36 12 2 +	96.39	1.0334	0.04
97.17	1.0271	5.6	32 20 6 +	97.10	1.0277	0.07
97.75	1.0226	6.3	29 25 3 +	97.76	1.0225	-0.01
98.15	1.0195	5.9	34 18 2 +	98.16	1.0194	-0.01
98.67	1.0155	5.9	36 14 2 +	98.70	1.0153	-0.03
99.48	1.0094	5.3	35 17 1 +	99.55	1.0089	-0.07
99.92	1.0061	5.3	39 1 1 +	99.90	1.0063	0.02
100.49	1.0020	28.3	32 16 16 *	100.49	1.0020	0.00
100.87	0.9992	7.9	38 10 0 +	100.85	0.9994	0.02
101.14	0.9973	5.6	36 16 0 +	101.21	0.9968	-0.07
101.33	0.9959	6.3	33 21 5	101.34	0.9958	-0.01
102.43	0.9882	8.6	29 27 3 +	102.42	0.9882	0.01
103.13	0.9834	5.3	37 15 1 +	103.14	0.9833	-0.01
103.53	0.9807	4.9	32 24 2 +	103.55	0.9805	-0.02
103.74	0.9793	4.9	40 2 2 +	103.73	0.9793	0.01
104.20	0.9762	4.6	33 23 1 +	104.23	0.9760	-0.03
104.61	0.9735	6.3	33 23 3 +	104.60	0.9736	0.01
105.39	0.9684	4.6	34 22 2 +	105.37	0.9685	0.02
106.09	0.9639	4.9	37 17 1 +	106.06	0.9641	0.03
106.57	0.9609	5.6	40 8 2 +	106.47	0.9615	0.10

106.89	0.9589	5.6	38 14 6 +	106.84	0.9592	0.05
107.22	0.9569	5.3	36 18 8 +	107.21	0.9569	0.01
107.49	0.9552	5.6	31 27 1 +	107.53	0.9550	-0.04
108.23	0.9508	4.9	41 5 1 +	108.28	0.9505	-0.05
109.25	0.9447	25.9	40 8 8 * +	109.25	0.9447	0.00
109.67	0.9423	8.9	34 24 2 +	109.63	0.9425	0.04
110.48	0.9376	5.6	35 23 1 +	110.52	0.9374	-0.04
110.74	0.9361	5.9	40 12 4 +	110.76	0.9361	-0.02
110.99	0.9347	4.6	38 16 8 +	110.94	0.9350	0.05
111.26	0.9332	4.9	39 15 5 +	111.28	0.9331	-0.02
111.57	0.9315	4.3	35 23 5 +	111.65	0.9310	-0.08
112.30	0.9275	4.6	39 15 7 +	112.42	0.9269	-0.12
112.48	0.9265	4.6	36 22 4 +	112.46	0.9266	0.02
112.67	0.9255	5.3	30 30 0 +	112.65	0.9256	0.02
113.21	0.9226	6.3	32 28 2 +	113.23	0.9225	-0.02
113.43	0.9215	6.3	30 30 4 +	113.42	0.9215	0.01
113.95	0.9187	4.9	33 27 3 +	113.95	0.9187	0.00
114.30	0.9169	5.6	37 21 5 +	114.34	0.9167	-0.04
114.86	0.9140	4.6	42 8 4 +	114.77	0.9145	0.09
115.09	0.9129	4.3	35 25 1 +	115.11	0.9128	-0.02
115.47	0.9110	4.3	43 3 1 +	115.50	0.9108	-0.03
116.31	0.9068	5.6	43 5 1 +	116.29	0.9069	0.02
118.52	0.8962	5.9	40 16 8	118.52	0.8962	0.00
118.92	0.8944	5.9	38 22 0 +	118.93	0.8943	-0.01
119.92	0.8898	7.2	31 31 5 +	119.89	0.8900	0.03
120.36	0.8879	5.6	44 4 2 +	120.35	0.8879	0.01
120.52	0.8871	4.9	42 14 0 +	120.55	0.8870	-0.03
120.91	0.8854	4.9	44 4 4 +	120.96	0.8852	-0.05
121.13	0.8845	4.9	39 21 3 +	121.11	0.8845	0.02
122.36	0.8792	5.3	37 25 1 +	122.36	0.8792	0.00
122.81	0.8773	4.9	40 20 2 +	122.83	0.8772	-0.02

125.20	0.8676	11.0	32 32 0 *	125.17	0.8677	0.03
125.75	0.8655	5.9	33 31 3 +	125.77	0.8654	-0.02
126.47	0.8627	5.9	34 30 4 +	126.48	0.8627	-0.01
126.81	0.8614	6.6	36 28 0 +	126.92	0.8610	-0.11
127.52	0.8588	7.6	35 29 5 +	127.52	0.8588	0.00
128.40	0.8556	5.6	37 27 3 +	128.42	0.8555	-0.02
129.11	0.8530	5.6	38 26 0 +	129.15	0.8529	-0.04
130.64	0.8477	5.3	39 25 1 +	130.71	0.8475	-0.07
131.36	0.8453	5.3	38 26 6 +	131.23	0.8457	0.13
132.23	0.8424	4.6	39 25 5 +	132.12	0.8428	0.11
132.63	0.8411	5.6	40 24 2 +	132.66	0.8411	-0.03
133.99	0.8368	5.9	33 33 5	134.05	0.8367	-0.06
136.37	0.8297	29.9	40 24 8 *	136.37	0.8297	0.00
137.07	0.8277	7.9	39 27 1 +	137.07	0.8277	0.00
138.79	0.8229	4.6	40 24 10 +	138.72	0.8231	0.07
139.84	0.8201	5.6	40 26 4 +	139.80	0.8203	0.04
140.61	0.8182	16.3	48 0 0 + *	140.63	0.8181	-0.02
141.38	0.8162	6.6	35 33 1 +	141.40	0.8162	-0.02
141.46	0.8160	7.6	34 34 2 +	141.47	0.8160	-0.01
142.25	0.8141	4.9	34 34 4 +	142.32	0.8139	-0.07
142.44	0.8136	4.9	37 31 1 +	142.54	0.8134	-0.10
144.25	0.8094	4.9	37 31 5 +	144.32	0.8092	-0.07
144.98	0.8077	4.6	39 29 1 +	144.93	0.8078	0.05
146.28	0.8049	4.9	38 30 6 +	146.25	0.8050	0.03
146.79	0.8038	4.9	39 29 5 +	146.81	0.8038	-0.02
148.30	0.8007	5.3	36 28 18	148.21	0.8009	0.09
148.75	0.7999	5.9	39 29 7 +	148.80	0.7998	-0.05
149.64	0.7981	5.6	40 28 6 +	149.57	0.7983	0.07

*13 stronger FCC lines come from the fluorite type basic sub-cell.

[#] Several of the stronger lines agree with all the indexing of stronger spots in the SAED patterns, (Laverov *et al.*, 2011a).

Figure captions

Figure 1. SAED pattern of M8 in the (1 1 0) plane of the reciprocal lattice.

Figure 2. X-ray diffraction pattern on a linear scale exemplifies how very weak are the superlattice lines, dominated by the sub-cell lines. The low angle, $2\theta = 2–10°$, is shown inset on a square root scale. Advantage accrues at low-angles where intensities are slightly enhanced by the $(1+\cos^2\theta)$ term in the usual scattering equation.

Figure 3. Expanded section of Figure 2 - (a), better to emphasize the many low intensity peaks from the superlattice on a square root scale. And - (b), in the region of (8 8 8), all peaks are M8 with minor impurities: P, pseudobrookite and Z, zirconolite; there are no visible peaks due to M3 or M5.

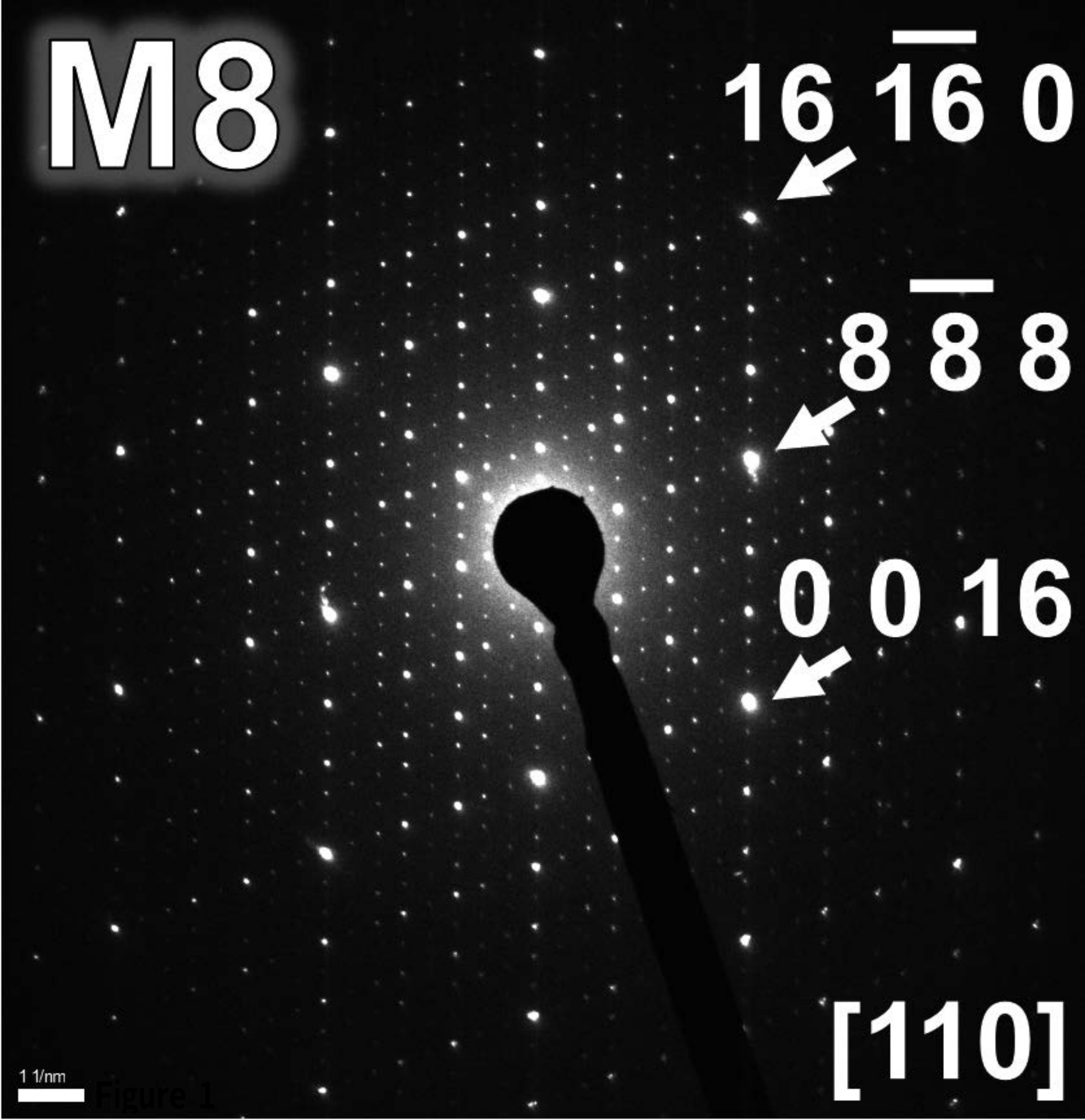

Figure 1

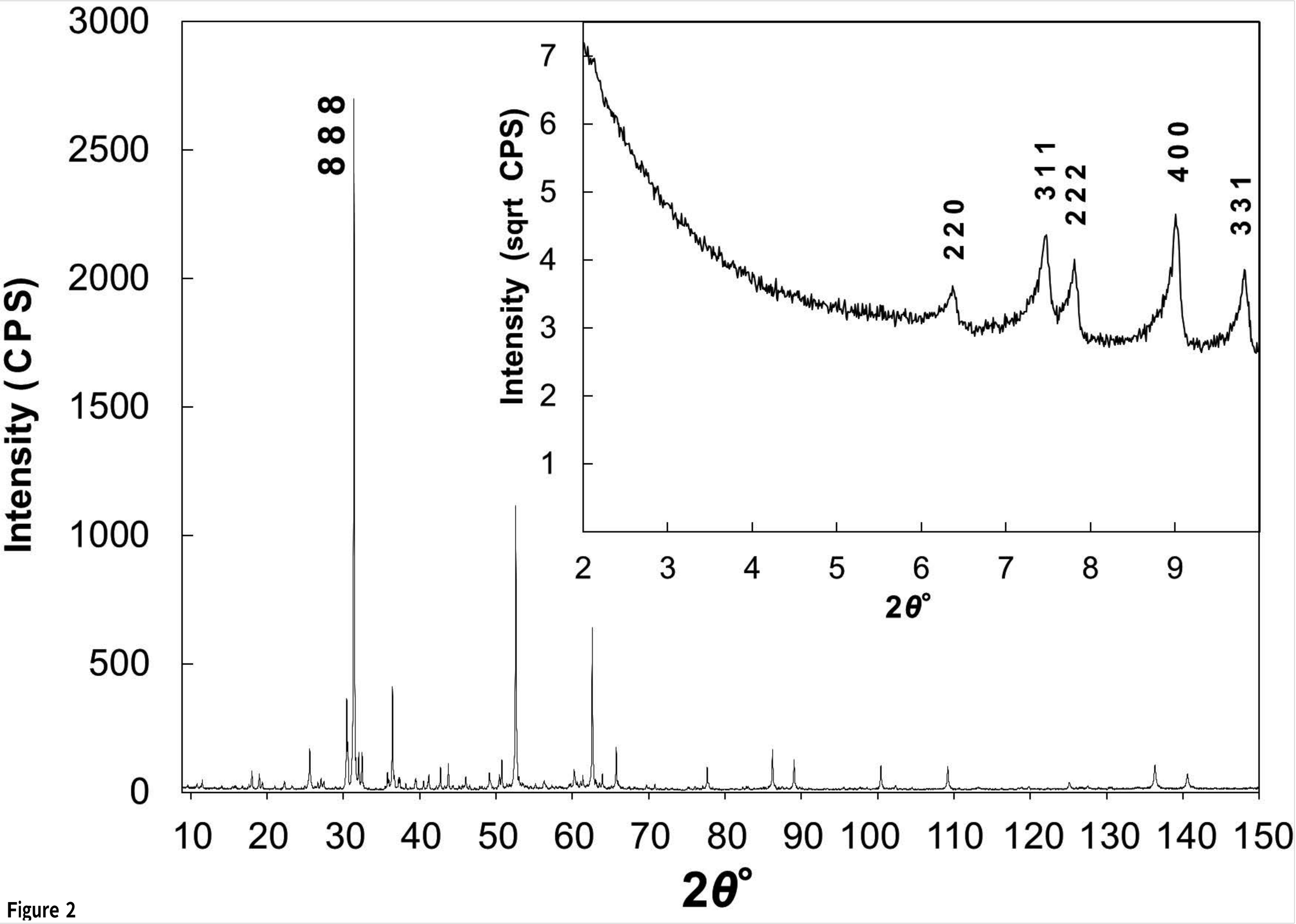
Intensity (CPS)
3000
2500
2000
1500
1000
500
0
8 8 8
10 20 30 40 50 60 70 80 90 100 110 120 130 140 150
2θ°
Intensity (sqrt CPS)
7
6
5
4
3
2
1
2 0
3 1 1
2 2 2
4 0 0
3 3 1
2 3 4 5 6 7 8 9
2θ°

Figure 2

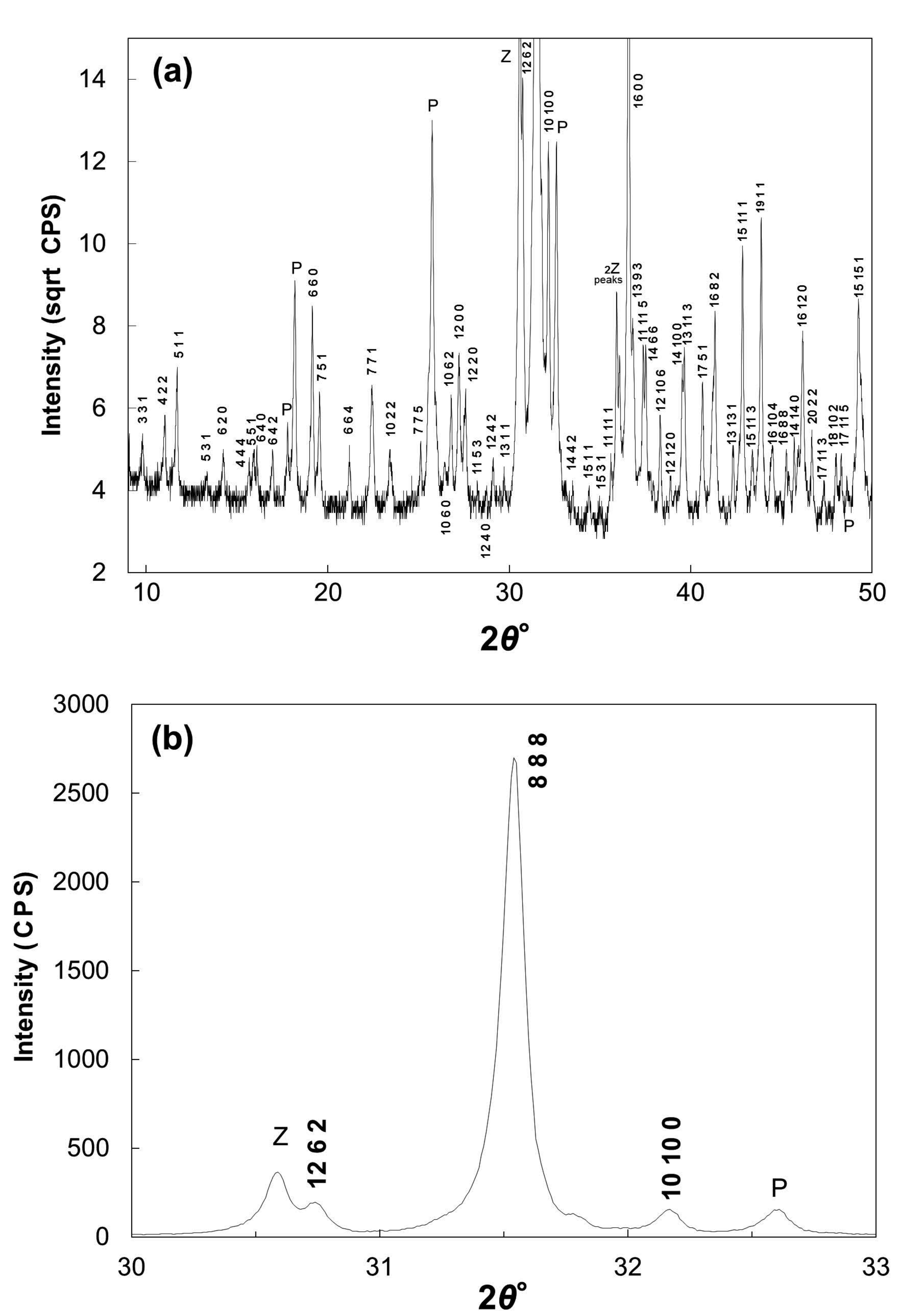

Figure 3